

Stable suspension and dispersion-induced transitions from repulsive Casimir forces between fluid-separated eccentric cylinders

Alejandro W. Rodriguez,¹ J. N. Munday,² J. D. Joannopoulos,¹
Federico Capasso,² Diego A. R. Dalvit,³ and Steven G. Johnson⁴

¹*Department of Physics, Massachusetts Institute of Technology, Cambridge, MA 02139*

²*Department of Applied Physics, Harvard University, MA 02139*

³*Theoretical Division, Los Alamos National Laboratory, Los Alamos, NM 87545*

⁴*Department of Mathematics, Massachusetts Institute of Technology, Cambridge, MA 02139*

Using an exact numerical method for finite-size nonplanar objects, we demonstrate a stable mechanical suspension of a silica cylinder within a metallic cylinder separated by ethanol, via a repulsive Casimir force between the silica and the metal. We investigate cylinders with both circular and square cross sections, and show that the latter exhibit a stable orientation as well as a stable position, via a method to compute Casimir torques for finite objects. Furthermore, the stable orientation of the square cylinder is shown to undergo an unusual 45° transition as the separation length-scale is varied, which is explained as a consequence of material dispersion.

The Casimir force, arising from quantum fluctuations of the electromagnetic field, was first described as an attractive, monotonically decaying force between metallic plates [1], but repulsive interactions can arise in special circumstances, e.g. involving fluid-separated asymmetric plates [2]. It has been proposed that repulsive Casimir forces between fluid-separated objects can lead to stable mechanical equilibria, and hence frictionless static bearings or other interesting passive-suspension devices [3, 4, 5]. However, previous calculations and experiments involving fluid-separated objects have been restricted to geometries involving parallel plates or approximations thereof [6] (similar to work on air-separated metals, as reviewed in several recent papers, e.g. Ref. 7). Here, using recently developed numerical techniques [8, 9], we present accurate theoretical calculations of Casimir forces/torques between fluid-separated objects with finite square and circular cross sections (Fig. 1 insets) that rigorously demonstrate stable positional/orientational Casimir equilibria [26]. (A similar geometry involving vacuum-separated perfectly-metallic circular cylinders has been solved analytically and shown to exhibit an unstable positional equilibrium [10].) In the case of square cross sections, further investigation of the stable orientational equilibrium with respect to rotations reveals a surprising result—the stable orientation changes by 45° depending on the length-scale, a feature that we show to be a consequence of material dispersion: for certain fluid-separated materials, the frequency dependence of the permittivity (material dispersion) causes the Casimir force to switch from repulsive to attractive at some critical separation [2]; this leads to the orientation transition described here, and may produce other length-scale-based qualitative transitions in future geometries. We present a method to compute Casimir torques on finite objects (in contrast to previous uncontrolled approximations [11] or analytical results for semi-infinite planes (half-spaces) [3, 12, 13]); we supplement

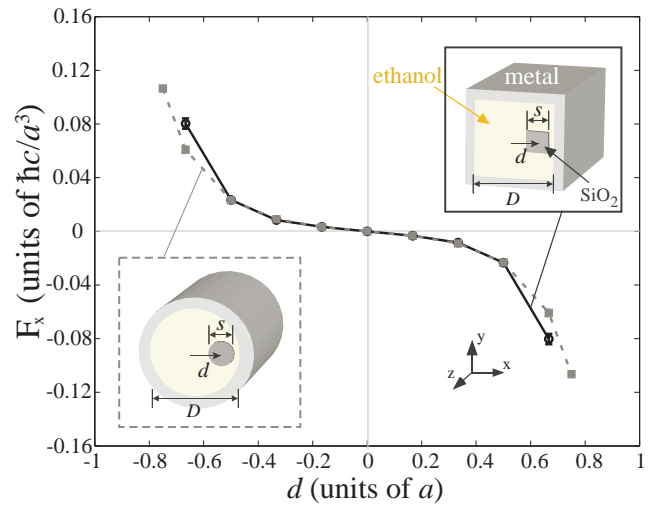


FIG. 1: Casimir force F_x in the x -direction, per unit z -length, on a silica cylinder suspended within a perfectly-metallic cylinder (inset), separated by fluid (ethanol), as a function of the x -displacement from equilibrium (eccentricity) d [in units of $a = 0.5(D - s)$] for both circular (solid-line) and square (dashed-line) cylinders. $d = 0$ is seen to be a stable equilibrium.

the accurate results with a heuristic model based on the proximity force approximation (PFA) that turns out to capture qualitative behaviors of the orientational transition, and therefore provides some simple insight.

A repulsive Casimir force arises between parallel plates of permittivity ϵ_1 and ϵ_2 separated by a fluid of permittivity ϵ_f , if $\epsilon_1(i\xi) < \epsilon_f(i\xi) < \epsilon_2(i\xi)$ for a sufficiently wide range of imaginary frequencies $\xi = \text{Im } \omega$ [2]. Three such materials are silica (SiO_2) and metal (Au) separated by ethanol [4], discussed in more detail below. We investigated the three-dimensional (constant cross-section) geometries shown in the inset of Fig. 1: square or circular SiO_2 cylinders of diameter s surrounded by a metal cylinder of diameter D , separated by ethanol.

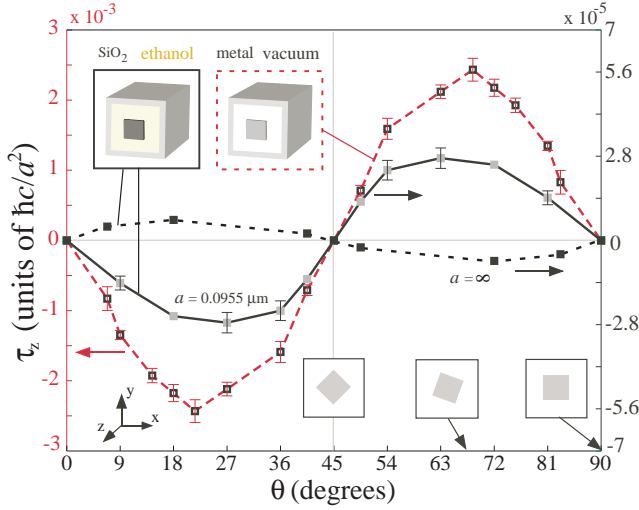


FIG. 2: Casimir torque τ_z , per unit z -length, on the inner square rod of eccentric square cylinders as a function of the angle θ with respect to the x -axis (see right insets) for two square cylindrical geometries depicted on the top insets (see text). Error bars are estimates of the effect of finite grid resolution.

For computational convenience, we use a perfect metal [$\varepsilon(i\xi) \rightarrow \infty$, corresponding to negligible skin depth] for the outer cylinder, but we use experimental ω -dependent permittivities for the SiO₂ and ethanol. In such geometries, with bodies of sizes and curvatures comparable to their separations, approximations of the Casimir force as a pairwise attraction between surfaces are not valid and their qualitative predictions (e.g. stability) may be incorrect [8, 16, 17].

Figure 1 shows the force per unit z -length on the inner cylinder as a function of the displacement from equilibrium d (eccentricity, or center-to-center cylinder separation) in units of a , where $a \equiv 0.5(D - s) = 0.0955 \mu\text{m}$ so that $d/a = \pm 1$ for touching surfaces, for parameters $s/D = 0.25$. It demonstrates a stable equilibrium with respect to displacements from $d = 0$ for both square (solid black) and circular (dashed grey) cross sections. The computational method employed here was introduced in Ref. 9, and is based on integration of the mean electromagnetic stress tensor (valid even for fluids [18]) evaluated in terms of the imaginary-frequency Green's function via the fluctuation-dissipation theorem [9]. Additional details on the calculation are provided below.

Having demonstrated positional stability (Fig. 1), we now explore an unusual effect arising from material dispersion. The square cylinder geometry (Fig. 2 inset) must, from symmetry considerations, exhibit two equilibrium orientations ($\theta = 0^\circ$ and $\theta = 45^\circ$). *A priori*, it is not clear which of the two configurations is stable, and under what circumstances. To answer these questions, Fig. 2 plots the Casimir torque per unit z -length on the inner square, as a function of the rotation angle

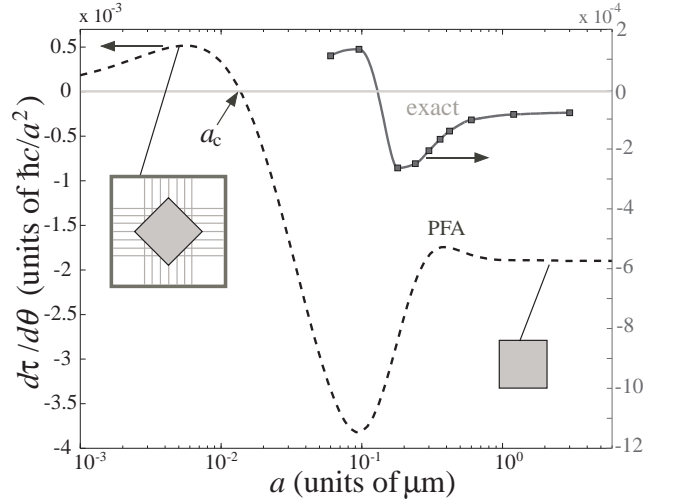


FIG. 3: Derivative of the Casimir torque in the z -direction with respect to θ , $d\tau_z/d\theta$, in units of $\hbar c/a^2$, evaluated at $\theta \approx 45^\circ$, as a function of length-scale $a = 0.5(D - s)$. The solid line is a fit to the exact Casimir torque, computed by our numerical method (solid squares), and the dashed line is the torque as computed by a PFA approximation. Both curves display a change (dispersion-induced transition) in the stable orientation of the square.

θ between the inner and outer squares. In addition to computing the torque for the stable equilibrium structure consisting of SiO₂-ethanol-perfect-metal (repulsive forces), we also analyze the torque when both cylinders are perfectly metallic and separated by vacuum, in which case the forces are purely attractive and there is no stable equilibrium with respect to displacements [10].

The resulting torque per unit z -length is shown in Fig. 2, for both the repulsive (solid, filled-square-lines) and attractive (solid, open-square-line) cases, as θ is varied from 0° to 90° . The stable orientation for both repulsive and attractive cases is $\theta = 45^\circ$, a surprising result considering the difference in the sign of the force. A stable orientation of 45° in the purely metallic case is not so surprising, since an attractive force that decreases with separation should intuitively (in the heuristic picture of pairwise attractions between surfaces) favor an orientation where the surfaces are as close as possible, hence pulling the corners of the inner square towards the outer surfaces. On the other hand, a repulsive force should intuitively push the surfaces as far apart as possible, which would seem to suggest a 0° stable orientation for the repulsive case. The reason for this apparent contradiction between intuition and the numerical results of Fig. 2 lies in the effects of material dispersion—as explained below, $\varepsilon_{\text{Si}} - \varepsilon_{\text{eth}}$ (and hence the force) switches sign at some lengthscales (some $1/\xi$). For example, if we neglect the frequency dispersion of SiO₂ and ethanol, and use only the $\xi \rightarrow 0$ dielectric constants, the torque as a function of θ (shown as the dashed black line in Fig. 2) indeed

exhibits a stable orientation at 0° , as expected from the simple pairwise intuition: in this case, the force is repulsive at *all* length-scales, since dispersion is absent.

Since $\theta = 0^\circ$ is unstable for the $a = 0.0955 \mu\text{m}$ fluid case and stable for $a \rightarrow \infty$ (equivalent to $\xi \rightarrow 0$), there *must* be a transition at some critical intermediate length-scale a_c . One way to determine a_c is to calculate the derivative of the torque on the inner cylinder at $\theta = 45^\circ$ as a function of a (noting that the dimensionless torque $\tau a^2/hc$ goes to a nonzero value as $a \rightarrow \infty$), and to look for a change in the sign. This derivative is plotted as the solid line in Fig. 3 and exhibits the expected transition from stable ($d\tau_z/d\theta > 0$, left) to unstable ($d\tau_z/d\theta < 0$, right) at $a_c \approx 0.1 \mu\text{m}$, a consequence of material dispersion. A better understanding of this transition can be gained by inspecting a simple heuristic (PFA). PFA is only an *ad hoc* model, in which the force on each point of the surface (and hence the torque) is treated as simply the parallel-plate (Lifshitz) force between fluid-separated half-spaces (with “lines of interaction” perpendicular to the outer surface, as depicted in the left inset of Fig. 3). This simple model turns out to capture some qualitative features of the orientation transition, as shown by the dashed line in Fig. 3, although it is of course quantitatively incorrect [13].

PFA provides an explanation for why orientational stability need not coincide with positional stability. Stability, in general, arises from the competing interactions of the inner and outer surfaces, e.g. in the 45° orientation for repulsive interactions, the nearest surface “pushes” the corner away, while the other surface “pushes” the corner back. Which of these competing forces dominates depends on their sign and power law, but in the torque $\boldsymbol{\tau} = \mathbf{r} \times \mathbf{F}$ case, there is an additional effect (which stems from the $\mathbf{r} \times$ dependence)—the force “from” the nearest surface elements is parallel to the radial direction and does not produce a torque, whereas it does contribute to the total force. Therefore, positional and orientational stability can respond differently to the same material dispersion, because the lengthscales of the dominant contributing separations differ. More generally, in the exact model where the force cannot be decomposed into additive contributions, the dominant imaginary-frequency contribution can differ between torque and force.

There is another interesting feature in Fig. 3: for $a > a_c$, the derivative of the torque is nonmonotonic, *decreasing* in magnitude towards $a \rightarrow \infty$. At first glance, this may be counter-intuitive because the dielectric contrast is maximum for $\xi \rightarrow 0$ (Fig. 4 inset), which would seem to predict greater forces. However, because the net torque arises from a competition between nearby and far-away surfaces, the magnitude depends not only on the force but also on the power law: if the force decreases more rapidly with distance, then faraway surfaces contribute less and the net torque is larger. This is precisely what is happening here, because at intermediate

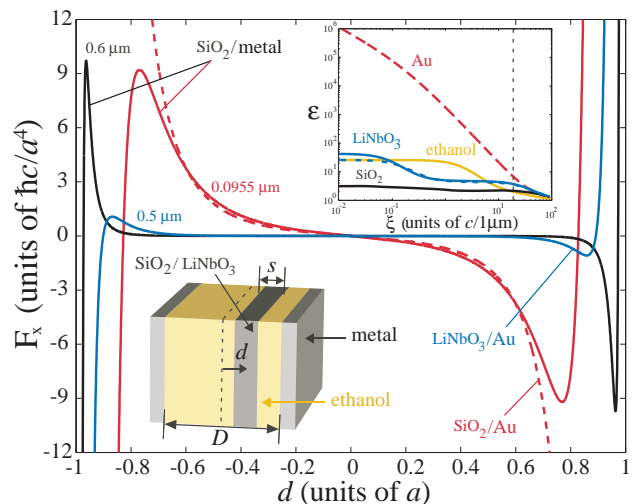


FIG. 4: Casimir force F_x in the x -direction, per unit area, between a planar silica slab suspended between two perfect-metal plates (solid red and black lines) or gold half-spaces (dashed red line), separated by a fluid (ethanol), as a function of the dimensionless x -displacement d from equilibrium. The force is plotted also at two length-scales $a \equiv 0.5(D-s) = 0.0955 \mu\text{m}$ (red lines) and $a = 0.6 \mu\text{m}$ (black line). The solid blue line shows the same quantity for the case of a lithium-niobate slab and a gold half-space, for $a = 0.5 \mu\text{m}$. (Insets:) Top inset: $\varepsilon(i\xi)$ for SiO_2 (black), LiNbO_3 (solid and dashed blue), ethanol (orange) and gold (red) as a function of imaginary frequency ξ . Bottom inset: schematic of geometry.

a , material dispersion acts to increase the power law [2] compared to the $a \rightarrow \infty$ case where dispersion plays no role. Preliminary work shows similar effects in the positional stability. This also explains the relative torque magnitudes for $a \rightarrow \infty$ and $a = 0.0955 \mu\text{m}$ in Fig. 2.

Since the qualitative behavior of the torque transition is captured by PFA, it makes sense to examine a simple one-dimensional model in detail, depicted on the inset of Fig. 4: a SiO_2 slab of thickness s , separated from two metallic half-spaces, a (surface-to-surface) distance $a \equiv 0.5(D-s)$ from the SiO_2 surface, with ethanol (fluid) in between. This geometry is analyzed using a generalization of the Lifshitz formula [19]. Figure 4 shows the force per unit area on the inner slab (again using $s/D = 0.25$), as a function of the displacement d , for two length-scales: $a = 0.0955 \mu\text{m}$ (red), and $a = 0.6 \mu\text{m}$ (black). There is a stable equilibrium at $d = 0$, just as for the two-dimensional case in Fig. 1. In the case of the perfectly-metallic half-spaces, the force changes sign at a critical distance d_c that depends on the length-scale a . However, if we assume the metallic half-spaces to be made out of the real metal gold (Au), shown by the dashed line for $a = 0.0955 \mu\text{m}$, this transition disappears, and the force is always repulsive. Both of these features are explained by the inset of Fig. 4, which shows $\varepsilon(i\xi)$ of SiO_2 , ethanol and Au. The key point is that the contributions to the Casimir force come primarily from

imaginary “wavelengths” $2\pi/\xi$ larger than some length-scale set by the separation, while very short wavelengths (large ξ) on this scale are exponentially cut off in the force integral [20]. So, for large length-scales a , the force is dominated by the small- ξ permittivities, which are in the correct order $\varepsilon_{\text{silica}} < \varepsilon_{\text{ethanol}} < \varepsilon_{\text{metal}}$ to obtain a repulsive force and a stable equilibrium. On the other hand, for small length-scales and separations, large- ξ contributions become more and more important, and at large ξ the ordering switches to $\varepsilon_{\text{silica}} > \varepsilon_{\text{ethanol}}$ (for $\xi > 2.3 \text{ c}/\mu\text{m}$, where the intersection point is marked by the vertical dashed line on the inset of Fig. 4), leading to attractive contributions to the force. For the case of the perfect metal, these attractive contributions are large enough to flip the sign of the total force for small separations, whereas for Au the attractive high- ξ contributions are suppressed by the diminishing $\varepsilon(i\xi)$ of the Au (as the three permittivities become equal, their force contribution vanishes) and the force remains repulsive. While the transition is absent in the SiO_2 -ethanol-Au configuration, we have calculated the force between ethanol-separated lithium-niobate LiNbO_3 and Au plates and found a sign transition at separations $\sim 0.05 \mu\text{m}$. This is illustrated in Fig. 4 (solid blue line); because LiNbO_3 ’s anisotropy greatly complicates the modeling, we used a PFA approximation based on summing the Lifshitz forces between semi-infinite Au and LiNbO_3 slabs (neglecting the finite LiNbO_3 thickness). The two principal values of the permittivity tensor of LiNbO_3 [21] are plotted in the inset. There are also transitions for ethanol-separated barium-titanate and calcite plates at separations $\sim 0.01 \mu\text{m}$ [3]. Since the LiNbO_3 -ethanol-Au and barium-ethanol-calcite cases are much more difficult to compute (the outer cylinder is not a perfect metal and LiNbO_3 is anisotropic), we focus on the SiO_2 -ethanol-metal case here, which exhibits similar qualitative behaviors.

The experimental permittivities of SiO_2 and ethanol were fit to a standard multiple-oscillator model [22] that is accurate over a wide range of infrared to ultraviolet wavelengths: $\varepsilon(i\xi) = 1 + \sum_{n=1}^N C_n \left[1 + (\xi/\omega_n)^2 \right]^{-1}$, in terms of parameters ω_n and C_n fit to experiments. The parameters we used are [21, 23]: ethanol ($N = 2$) $\omega_n = \{6.6, 114\} \times 10^{14} \text{ Hz}$ and $C_n = \{23.84, 0.852\}$; SiO_2 ($N = 3$) $\omega_n = \{0.867, 1.508, 203.4\} \times 10^{14} \text{ Hz}$ and $C_n = \{0.829, 0.095, 1.098\}$. We model the dielectric constant of Au by the usual Drude model $\varepsilon(i\xi) = 1 + \omega_p^2/(\xi(\xi + \gamma))$, where $\omega_p = 1.367 \times 10^{14} \text{ Hz}$ and $\gamma = 5.320 \times 10^{13} \text{ Hz}$ [21]. The Casimir force \mathbf{F} is computed as an integral of the form $\mathbf{F} \sim \int_0^\infty d\xi \oint \langle \mathbf{T} \rangle d\mathbf{A}$ [9], where the mean stress tensor $\langle \mathbf{T} \rangle$ is computed at each position and frequency from the Green’s function as described in Ref. 9. The Casimir torque $\boldsymbol{\tau}$, was computed in the same framework, with a minor modification, $\boldsymbol{\tau} \sim \int_0^\infty d\xi \oint \mathbf{r} \times (\langle \mathbf{T} \rangle d\mathbf{A})$, also proposed in our earlier work [9].

We are hopeful that the phenomena described in this

paper will be amenable to experiment, since despite this nonplanar geometry, they have some advantages over planar geometries: the concentric configuration is a stable equilibrium, static charges on the outer metallic cylinder are screened in the interior, and the equilibrium is easily distinguished from electrostatic effects (which cannot produce stability [16]). (If we inverted the geometry, to have the silica on the outside and the metal on the inside, then the larger static permittivity of the fluid compared to the silica would lead to a classical stable equilibrium for a charged inner cylinder [16, 24, 25].) We expect that a similar stable equilibrium will be obtained for real metals, as in our one-dimensional calculation with Au in Fig. 4. As noted above, there are a number of materials that exhibit repulsive-attractive transitions (unlike SiO_2 -ethanol-Au), and they should therefore display the orientational transition. Our calculations have also uncovered an intriguing question to explore in future work: in the PFA heuristic, it appears that the critical lengthscale at which the orientational transition occurs is *smaller* than the corresponding positional transition lengthscale (changing from stable to unstable suspension), whereas the exact calculations give the opposite result.

This work was supported in part by U. S. Department of Energy Grant No. DE-FG02-97ER25308, the NSF MRSEC program under Grant No. DMR-0213282, and by the MIT Ferry Fund.

-
- [1] H. B. G. Casimir, Proc. K. Ned. Akad. Wet. **51**, 793 (1948).
 - [2] I. E. Dzyaloshinskii, E. M. Lifshitz, and L. P. Pitaevskii, Adv. Phys. **10**, 165 (1961).
 - [3] J. N. Munday, D. Iannuzzi, Y. Barash, and F. Capasso, Phys. Rev. A **71**, 042102 (2005).
 - [4] F. Capasso, J. N. Munday, D. Iannuzzi, and H. B. Chan, IEEE J. Selected Topics in Quant. Elec. **13**, 400 (2007).
 - [5] D. Iannuzzi, J. Munday, and F. Capasso, US Patent Application US20070066494 (2006).
 - [6] J. N. Munday and F. Capasso, Phys. Rev. A **75**, 060102(R) (2007).
 - [7] M. Bordag, U. Mohideen, and V. M. Mostepanenko, Phys. Rep. **353**, 1 (2001). K. A. Milton, Journal of Physics A: Mathematical and General **37**, R209 (2004). S. K. Lamoreaux, Rep. Prog. Phys. **68** (2005).
 - [8] A. Rodriguez, M. Ibannescu, D. Iannuzzi, F. Capasso, J. D. Joannopoulos, and S. G. Johnson, Phys. Rev. Lett. **99**, 080401 (2007).
 - [9] A. Rodriguez, M. Ibannescu, D. Iannuzzi, J. D. Joannopoulos, and S. G. Johnson, Phys. Rev. A **76**, 032106 (2007).
 - [10] D. A. R. Dalvit, F. C. Lombardo, F. D. Mazzitelli, and R. Onofrio, Phys. Rev. A **74**, 020101(R) (2006).
 - [11] A. Scardicchio and R. L. Jaffe, Nuclear Physics B. **704**, 552 (2005).
 - [12] S. J. van Enk, Phys. Rev. A **52**, 2569 (1995).
 - [13] R. B. Rodrigues, P. A. Maia Neto, A. Lambrecht, and S. Reynaud, Europhys. Lett. **75**, 822 (2006).

- [14] C.-G. Shao, A.-H. Tong, and J. Luo, Phys. Rev. A **72**, 022102 (2005).
- [15] H. Razmi and S. M. Modarresi, Int. J. Theor. Phys. **44**, 229 (2005).
- [16] D. A. R. Dalvit, F. C. Lombardo, F. D. Mazzitelli, and R. Onofrio, Europhys. Lett. **67**, 517 (2004).
- [17] H. Gies and K. Klingmuller, Phys. Rev. Lett. **96**, 220401 (2006).
- [18] L. P. Pitaevskiĭ, Phys. Rev. A **73**, 047801 (2006).
- [19] M. S. Tomaš, Phys. Rev. A **66**, 052103 (2002).
- [20] E. M. Lifshitz, Sov. Phys. JETP **2**, 73 (1956).
- [21] L. Bergstrom, Adv. Colloid and Interface Science **70**, 125 (1997).
- [22] J. Mahanty and B. W. Ninham, *Dispersion forces* (Academic London, 1976).
- [23] A. Milling, P. Mulvaney, and I. Larson, J. Colloid and Interface Science **180**, 460 (1996).
- [24] R. Y. Chiao and J. Boyce, Phys. Rev. Lett. **73**, 3383 (1994).
- [25] P. W. Milonni, D. F. V. James, and H. Fearn, Phys. Rev. Lett. **75**, 3194 (1995).
- [26] Here, we focus strictly on Casimir forces and ignore external forces such as gravity. We consider only static situations, so viscous forces are not present, nor is surface tension important for rigid immersed objects.